

MRI Evaluation of RF Ablation Scarring for Atrial Fibrillation Treatment

Yuri Ishihara¹, Reza Nazafat², John V. Wylie², Marius G. Linguraru¹, Mark E. Josephson²,
Robert D. Howe¹, Warren J. Manning², Dana C. Peters²

¹Division of Engineering and Applied Sciences, Harvard University, Cambridge, MA 02138 USA

²Cardiovascular-Division, Beth Israel Deaconess Medical Center, Harvard Medical School, Boston
MA 02215 USA

ABSTRACT

This study presents a multi-modality image registration method that evaluates left atrial scarring after radiofrequency (RF) ablation for pulmonary vein (PV) isolation. Our group has recently developed a delayed enhancement magnetic resonance imaging (DE-MRI) method with the potential to visualize and monitor non-invasively post-ablation scarring in the left atrium and the PV ostia. We wished to compare the 3D configuration of scarring in the DE-MRI image and the ablation points recorded by electroanatomical mapping (EAM) system, hypothesizing that scarring detected by DE-MRI overlaps with ablation points recorded by the EAM system used in the procedure.

Methods and Results: Three data sets, DE-MRI images and pulmonary vein MR angiography (PV-MRA) images, and EAM data (CARTO-XP, Biosense-Webster, Inc., Diamond Bar, CA) from a patient who underwent PV ablation, were used for the multi-modal image registration. Contrast-enhanced MR imaging was performed 38 days after the ablation procedure. PV-MRA and DE-MRI were fused by intensity-based rigid registration. Scar tissue was extracted from the DE-MRI images using multiple threshold values. EAM data was further fused with segmented PV-MRA by the iterative closest point algorithm (ICP). After registration, the distance from PV-MRA to the scar was 2.6 ± 2.1 mm, and from ablation points to the surface of the scar was 2.5 ± 2.3 mm. The fused image demonstrates the 3D relationship between the PV ostia, the scar and the EAM recording of ablation points.

Conclusion: Multimodal data fusion indicated that the scar tissue lesion after PV isolation showed good overlap with the ablation points.

Keywords: Cardiac procedure, MRI, Pulmonary Vein Isolation, Iterative Closest Point, Image Fusion, Image-guided therapy, Validation, Atrial fibrillation

1. INTRODUCTION

Pulmonary vein (PV) isolation by radiofrequency (RF) ablation is an effective minimally invasive treatment for atrial fibrillation (AF). AF is the most common clinical arrhythmia, and is characterized by disorganized atrial activation that results in significant morbidity and health care expenditures. Over 90 percent of entopic foci that initiate AF originate from the PV. An estimated 2.2 million people in North America have AF, which is a major cause of stroke (1).

During catheter ablation of AF, fluoroscopic and intracardiac echocardiographic guidance is used to position a catheter against regions of PV ostia. RF energy is applied to disrupt tissue integrity and isolate the PV electrically. Sensors in the catheter can record the tip position using electromagnetic tracking and provide electro-anatomical mapping (EAM) of action potential timing and amplitude. This system significantly reduces fluoroscopy time and procedure time compared to fluoroscopy alone. During long-term follow up, approximately 10-27 % of patients experience recurrence AF (1). The mechanisms for failure from previously isolated PVs are not fully understood. One hypothesis is that the scar is circumferentially incomplete and cannot successfully inhibit electrical conductivity originated from PV. Costly, repeat invasive electrophysiological studies are then performed. Cardiovascular magnetic resonance imaging (CMR) is frequently used in RF ablation therapy, for pretreatment planning and post treatment evaluation of pulmonary vein stenosis. 3D visualization of the anatomy of the PV-LA region is required by the electrophysiologists for understanding highly variable patient-specific anatomies. This information can be provided by contrast-enhanced 3D magnetic resonance angiography (MRA).

We developed a high-resolution 3D delayed enhancement MRI (DE-MRI) technique for visualization of scar tissue around the PVs after RF ablation (2), in which scar is bright because of delayed contrast agent accumulation in scarred ablated tissue. The complex 3D anatomy of the PV-LA area requires visualization tools in order to understand the scarring and its relationship to the PV ostia and LA and to assess the spatial configuration and continuity of scarring. In addition, the location of scar tissue from DE-MRI images can be compared with ablated points recorded from catheter EAM during RF ablation to assess the effectiveness of this intra-procedure guidance. This promises to be a significant means of evaluating outcomes of the treatment and optimizing the treatment system to reduce side effects and increase efficacy. This DE-MRI data permits, for the first time, the comparison of scar as observed by MR to the ablated points recorded by catheter tracking system during RF ablation.

Since the DE-MRI images represent the locations of scar, and the EAM data represent the recorded ablation sites, we are investigating the extent to which the scar image detected by DE-MRI overlaps with ablation points recorded by the EAM system. Although the end-point for RF ablation therapy is electrical isolation of the PVs, non-contiguous ablation sites may indicate a non-ideal ablation pattern. To test this hypothesis, we developed registration methods among multiple image modalities, namely PV-MRA, DE-MRI, and EAM data sets. The iterative closest point algorithm (ICP) (3), a surface registration method, was used to register EP catheter points and corresponding 3D surface points from PV-MRA. We overlaid the scar image onto the PV-MRA for an effective 3D visualization, and further superimposed the recorded ablation points into the fused image.

2. METHODS

We have developed a multimodality data fusion method. The overall image fusion technique is described in Figure 1. First, intensity-based rigid body transformation was calculated between DE-MRI and PV-MRA images. Then the scar tissue volume was extracted from DE-MRI. Next, a transformation between PV-MRA and EAM was calculated by ICP. Finally, scar volume, PV-MRA, and EAM data were fused using the computed transformations. Once we obtained the all data sets in the same coordinate system, the scar image, EAM ablation points were overlaid on the PV-MRA image for visualization.

2.1 Data Sets

The study population consists of over 50 patients who have undergone RF-ablation of PVs, using catheter-guidance. Each patient has complete sets of data, namely: (1) post-treatment scar image (average 45 days after ablation) using DE-MRI (Figure 2); (2) post-treatment conventional contrast enhanced PV-MRA of the pulmonary vessels; (3) ablation points recorded by the CARTO system (Biosense-Webster, Inc., Diamond Bar, CA). One patient was selected for this initial data fusion study.

2.1.1 PV-MRA imaging

Conventional contrast enhanced MRA of the PV and LA, using breath-hold (end-expiratory) non-ECG-gated 3D spoiled gradient imaging was acquired during the first pass of 0.2 mmol/kg Gd-DTPA using a 1.5 Tesla MR imaging system (Achieva, Philips Medical System, Best, The Netherlands).

2.1.2 DE-MRI

A 3D navigator-gating (end-expiratory), and ECG-gated (end-diastolic) inversion-recovery segmented gradient echo sequence was performed 20 minutes after administration of 0.2mmol/kg of the Gd-DTPA injection (Figure 2) (2).

2.1.3 EAM data

Anatomical points and ablation points from the ablation catheter (8 mm NaviStar, Biosense Webster, Diamond Bar, CA) were recorded by the electromagnetic mapping system (CARTO-XP, Biosense-Webster, Diamond Bar, CA). First, LA and PVs were mapped by collecting points while the catheter was placed in each region and individually labeled. The NaviStar catheter was deployed inside each PV and slowly pulled back to the LA and multiple PV points were sampled during this process. Then ablation points were manually recorded when designated by the electrophysiologist following the standard procedure protocol. The recorded catheter tip locations (x, y, z coordinates) were sampled at atrial end-diastole. The system records the (x, y, z) coordinates of each point mapped in the LA, in the PVs and each ablation site. The anatomical representation of the data set provided by the system is shown in Figure 3.

2.2 Image processing and Image registration

2.2.1 Scar volume extraction

The scar tissue area was extracted from DE-MRI. First, we selected PV-atrial area on the scar DE-MRI to exclude locations outside of the LA and PV wall in each DE-MRI slices. Then a threshold was set at blood signal + 1, 2, 3, 4, 5, 6, and 7 standard deviations (STD) above noise signal, to test each threshold level. The threshold levels were evaluated visually to determine the best threshold value. Finally, small unconnected components were removed. Matlab 2006a (Math Works, Natick, MA) was used for all image processing and image registration.

2.2.2 Segmentation of PV-MRA

A high contrast PV-MRA image was used for anatomical segmentation of PVs. The vascular structures were segmented by setting a threshold and saved as a binary volume data set. These vascular structures include PVs, pulmonary artery, cardiac chambers, and the aorta. Components smaller than 50,000 voxels were eliminated. The large components were removed by hand segmentation slice by slice then the small elements less than 50,000 voxels were again eliminated. Small parts including the aorta were eliminated by keeping large connecting components and then the surface points on the LA-PV area were obtained.

2.2.3 PV-MRA/DE-MRI registration

Post-treatment PV-MRA and DE-MRI scar image before the segmentation were co-registered using intensity based rigid registration and transformation between the two data sets was determined. The sum of square difference in intensities was used as a cost function. A 2D-2D registration slice-by-slice was done first (Figure 4) and then the translation in z axis was computed using location information in the image header. We assumed negligible patient movement between PV-MRA and DE-MRI image because both images were obtained in the same scanning session. Further shift in the z -axis was evaluated by 3D visualization of scar volume and PV-MRA fusion. The transformation obtained from intensity based registration was used for registration between PV-MRA and scar volume segmented from DE-MRI.

2.2.4 EAM-PV-MRA registration

A total of 288 points recorded by the EAM system (labeled as points in the LA, points along the five PV branches, and ablation points) were used for EAM-(PV-MRA) registration. The registration was achieved in two steps. The first step was a coarse registration using landmarks. Three anatomical landmarks were chosen at junctions of the LA and left superior (LS) PV, left inferior (LI) PV, and right inferior (RI) PV. The 3D scatter plot of the EAM data was used to select the closest points for each PV branch (Figure 5). The corresponding points on the 3D surface model of PV-MRA were selected. The rigid body transformation between these three chosen landmarks on each data set was computed using singular value decomposition (SVD) (4).

The second step was a surface registration. The coarse transformation obtained from the first step was applied to the EAM data sets. The MRI coordinate system was converted into EAM's physical coordinate system. Then, the iterative closest point (ICP) algorithm (3) was applied to find the best matched surface registration (3). The transformation obtained was applied to the coarsely transformed EAM data.

3. RESULTS

3.1 PV-MRA segmentation for surface registration

Threshold based segmentation for the LA-PV area was effectively performed. The patient had five PVs. The anatomical representation of each PV and LA area was well demonstrated by the 3D visualization tool. There were 43,306 surface points extracted from this image, and closest points were found for the 288 points in the EAM data set

3.2 EAM/PV-MRA fusion

The average distance between EAM points and the PV-MRA surface was calculated to quantify the registration error. Average distance between all PV plus LA points recorded by EAM to PV-MRA surface points were 2.5 ± 2.8 mm (Table 1 and Figure 6). The LS contained one outlier and resulted in a high standard deviation (2.7 ± 7.0 mm).

Table 1. Distance between labeled anatomical structure recorded by EAM system and PV-MRA surface.

LA-PVs	LA	LI	LS	RS1	RS2	RI
2.5 ± 2.8 mm	1.3 ± 2.1 mm	1.3 ± 0.9 mm	2.7 ± 7.0 mm	1.6 ± 1.3 mm	1.2 ± 0.5 mm	2.5 ± 1.4 mm

Table 2. Distance between ablation points and DE-MRI scar surface to PV-MRA surface

ablation points to PV MRA surface (mm)	DE-MRI scar surface to MRA surface (mm)
2.6 ± 1.7 mm	2.6 ± 2.1mm

By neglecting this outlier, the histogram indicated that the LA has the highest error and standard deviation from PV-MRA surface (2.8±2.1 mm). Without outlier, the average distance between total EAM points and PV-MRA was reduced to 2.4 ± 1.9 mm. Distance between individual PV branches were followings: LI: 1.3±0.9; LS: 2.7±7.0 (without outlier 1.3 ± 0.8); RS1: 1.6±1.3; RS2: 1.2±0.5; RI: 2.5±1.4 (Figure 6). The mean distance between PV-MRA surface and ablation points was 2.6 ± 1.7 mm. The histogram served as a metric of ablation points/PV-MRA registration error; 50% of the points had less than 2.2 mm error, and 90% were within 4.7 mm.

3.3 DE-MRI scar/EAM data

Different threshold values for extracting scar image were plotted in Figure 7 with ablation points. 4STD was chosen as the optimum threshold by visual inspection and used in the rest of the analysis. The histogram of distance between ablation points to scar (mean blood + 4STD air) surface is plotted in Figure 8. The mean distance is 2.5 ± 2.3 mm. 50% of points had less than 1.7 mm, and 90% were within 5.5 mm. The histogram indicated that the ablation points and scar surface are closely related.

3.4 DE-MRI scar/PV-MRA surface

The distance between scar with threshold at blood + 4 STD air and PV-MRA surface is shown in Figure 8 and Table 2 (2.6 ± 2.1). 50% of points had less than 2.0 mm, 90% of points were within 5.5 mm.

3.5 DE-MRI/PV-MRA/EAM data fusion

The initial landmark based registration followed by ICP registration provided an excellent match for each PV, as demonstrated in Figure 9 and 10. Ablation points were visually confirmed around and within the scar tissue. Table 1 shows the distance between ablation points and PV-MRA surface.

4. DISCUSSION

In this report, we demonstrate for the first time the 3D visualization of the relationship between post-ablation scar tissue detected by DE-MRI and ablation points recorded by an EAM system (Figure 10). The relationship between the recorded ablation points, scar and the left atrial and pulmonary vein anatomy are effectively visualized by the 3D visualization tool. Ablation points recorded by the EAM system demonstrated a high correlation with the scar tissue. These results demonstrate that the scar tissue visualization by DE-MRI potentially is an effective non-invasive method of evaluating ablation treatment.

The mechanism of recurrence of AF after the PV isolation procedure is not well understood. One hypothesis is that the lesions created by RF ablation are non-continuous and thus fail to fully block ectopic electrical conductivity originating from the PVs. The complex geometry of the PVs requires a 3D visualization of the scar relative to the anatomy, because 2D visualization (e.g. slice by slice) is hard to interpret. The registration methods developed here will enable the assessment of the circumferential completeness of the PV ablations, using 3D visualization. The mismatch between intended ablation sites, and the ablation pattern visualized by DE-MRI, and its relationship to the PV ostia may be related to inaccuracies of the ablation system. The registration methods here allow for spatial comparison of scar formation detected by DE-MRI and intended ablation sites.

Our multi-modality data fusion method may serve as an aid to detect gaps around the PVs and locations where incomplete electrical block occurs. It could be useful for repeat procedures by providing electrophysiologists with the locations of prominent gaps.

4.1 EAM/PV-MRA registration

ICP was effective for registration of the EAM data points and the surface model extracted from PV-MRA, as previously demonstrated (5). Our results suggest that a close value for the initial (landmark-based) registration is essential (Figure 10). However, whether the result converges to true solution is unclear. The accuracy of ICP registration must be investigated by a phantom study. The scaling error between recorded points and physical distance also could be confirmed in a phantom study.

We measured the distance between the PV-MRA surface and the EAM points consisting of locations PV branches, and the left atrial surface, but excluding points which were ablation sites. The average distance between EAM and PV-MRA was 2.5 ± 2.8 mm. This is comparable to other studies (6). The LA had the highest error and standard deviation from PV-MRA surface. This indicates that the LA wall is likely to have greater freedom of motion compared to the PVs, which are more constrained.

Next we measured the mean distance between PV-MRA surface and EAM ablation points only (excluding other non-ablation sites) was 2.6 ± 1.7 mm (Table 2), again comparable to other studies (6). There are a number of potential reasons for registration errors, involving non-rigid body changes. The PV-MRA is obtained on a different day than the actual ablation procedure, so the position, organ motion, and fluid status of the patient might result in deformation. Manipulations of the catheter within the cardiac chamber during the procedure further introduce deformation of the LA wall and PV branches and result in ablation points being located further outside of the imaged vessel wall. Furthermore, the current PV-MRA protocol does not include ECG-gating. The pulmonary vein changes in size and location throughout the cardiac cycle (7); therefore a ECG-gated PV-MRA will potentially decrease registration error associated with cardiac cycle effects (8). There is uncertainty about catheter contact with the PV or LA wall during the recording of an ablation point. Furthermore, the process of recording ablation sites during PV isolation is not automatic but manual, and some timing errors (between time of ablation, and time of recording ablation) may result in errors in recorded ablation location. Lastly, the patient is on a respirator during the ablation procedure, but the PV-MRA is performed with a breath-hold. This also introduces registration errors.

4.2 DE-MRI scar/EAM registration

The minimum distance between ablation sites and the closest voxel of scar for multiple thresholding values were tested. However, it could not be used to choose an optimal threshold value, because it is minimized if the entire surface area of the LA is classified as scar. Therefore, we selected the best threshold visually as 4 STD above the blood signal. The distance between ablation points and scar for 4STD above blood signal was 2.5 ± 2.3 mm. The order of the error was similar to that of EAM/PV-MRA and DE-MRI/PV-MRA. In the future, we will attempt to quantify overlap volume of the scar by DE-MRI and the ablation sites that are dilated to a 5.5 – 6.4mm sphere as the “ideal” configuration of an ablation scar (9, 10) as a metric to further optimize the threshold value.

4.3 DE-MRI scar/PV-MRA registration

As described earlier, the scar volumes are highly influenced by the level of thresholding; therefore the distance measurement between scar volume and PV-MRA surface does not serve as a measuring tool of registration error between PV-MRA and DE-MRI. Our intensity based rigid registration was implemented only with three degree of freedom (x , y , and z shift) in translation and rotation along the z axis for individual slices. More robust 3D-3D registration needs to be developed in the future. To improve the registration error between segmented PV and scar tissue, again an ECG-gated PV-MRA would be helpful.

4.4 Evaluation of CARTO Merge systems using the DE-MRI scar/EAM registration method.

Systems that merge CT (6, 11) or MRI (5) anatomical images with the EAM system are increasingly available as a commercial product (e.g. CARTO Merge, Biosense Webster). This system imports pre-procedural CT or MRI images and potentially improve efficacy of the procedure by providing better representation of the vasculature during the procedure. Our DE-MRI method, fused with the EAM data could enable comparison of EP procedures guided by CARTO Merge with procedures guided by EAM alone, by comparing the scar location to the intended ablation sites.

4.5 Limitation of DE-MRI scar image

The DE-MRI acquisition suffers from several limitations. Motion blurring of the very thin atrial wall can reduce scar visualization. The DE-MRI uses 4 mm axial slices, which may be too thick to visualize PVs which are oriented in the superior-inferior direction (e.g. the left superior PV). Scar must be extracted with using manually intensive and user-dependent regions of interest on each slice, since not only scar tissue but also neighboring connective tissue such as the valves, and the aortic wall enhance.

Our DE-MRI technique is based on contrast enhanced MRI that has been shown to be an effective method for detection of myocardial infarctions (12, 13). Lesions after RF ablation in myocardium have been successfully visualized by Gd-enhanced MRI (10) in animal studies, but DE-MRI for RF ablation of the LA has not been validated in animals.

ACKNOWLEDGEMENTS

This work was supported by Grant No. NIH K01EB004434-02 and NIH R01 HL073647-01. The authors thank Dr. Williams Wells, Dr. Randy Ellis, Dr. Douglas Perrin, and Mr. Peter Hammer for their technical support.

REFERENCES

1. Fuster V, Ryden LE, Cannom DS, et al. ACC/AHA/ESC 2006 guidelines for the management of patients with atrial fibrillation-executive summary: A report of the American College of Cardiology/American Heart Association Task Force on practice guidelines and the European Society of Cardiology Committee for Practice Guidelines (Writing Committee to Revise the 2001 Guidelines for the Management of Patients with Atrial Fibrillation) Developed in collaboration with the European Heart Rhythm Association and the Heart Rhythm Society. *Eur Heart J* 2006;27(16):1979-2030.
2. Peters DC, Wylie JV, Botnar RM, et al. Detection of pulmonary vein and left atrial scar after catheter ablation using 3D navigator-gated delayed enhancement magnetic resonance imaging - initial experience. *Radiology* 2007;In Press.
3. Besl PJ, McKay ND. A Method for Registration of 3-D shapes. *IEEE Trans Pattern Analysis and Machine Intelligence* 1992;14(2):239-56.
4. Arun KS, Huang TS, Blostein SD. Least-square fitting of two 3-D point sets. *IEEE Trans Pattern Analysis and Machine Intelligence* 1987;PAMI-9(5):598-700.
5. Malchano ZJ, Neuzil P, Cury RC, et al. Integration of cardiac CT/MR imaging with three-dimensional electroanatomical mapping to guide catheter manipulation in the left atrium: implications for catheter ablation of atrial fibrillation. *J Cardiovasc Electrophysiol* 2006;17(11):1221-9.
6. Dong J, Calkins H, Solomon SB, et al. Integrated electroanatomic mapping with three-dimensional computed tomographic images for real-time guided ablations. *Circulation* 2006;113(2):186-94.
7. Lickfett L, Dickfeld T, Kato R, et al. Changes of pulmonary vein orifice size and location throughout the cardiac cycle: dynamic analysis using magnetic resonance cine imaging. *J Cardiovasc Electrophysiol* 2005;16(6):582-8.
8. Katoh M, Bucker A, Muhlenbruch G, Schauerte P, Gunther RW, Spuentrup E. Impact of ECG gating in contrast-enhanced MR angiography for the assessment of the pulmonary veins and the left atrium anatomy. *Rofo* 2006;178(2):180-4.
9. Deneke T, Khargi K, Muller KM, et al. Histopathology of intraoperatively induced linear radiofrequency ablation lesions in patients with chronic atrial fibrillation. *Eur Heart J* 2005;26(17):1797-803.
10. Dickfeld T, Kato R, Zviman M, et al. Characterization of radiofrequency ablation lesions with gadolinium-enhanced cardiovascular magnetic resonance imaging. *J Am Coll Cardiol* 2006;47(2):370-8.

11. Kistler PM, Rajappan K, Jahngir M, et al. The impact of CT image integration into an electroanatomic mapping system on clinical outcomes of catheter ablation of atrial fibrillation. *J Cardiovasc Electrophysiol* 2006;17(10):1093-101.
12. Wagner A, Mahrholdt H, Holly TA, et al. Contrast-enhanced MRI and routine single photon emission computed tomography (SPECT) perfusion imaging for detection of subendocardial myocardial infarcts: an imaging study. *Lancet* 2003;361(9355):374-9.
13. Croisille P, Revel D, Saeed M. Contrast agents and cardiac MR imaging of myocardial ischemia: from bench to bedside. *Eur Radiol* 2006;16(9):1951-63.

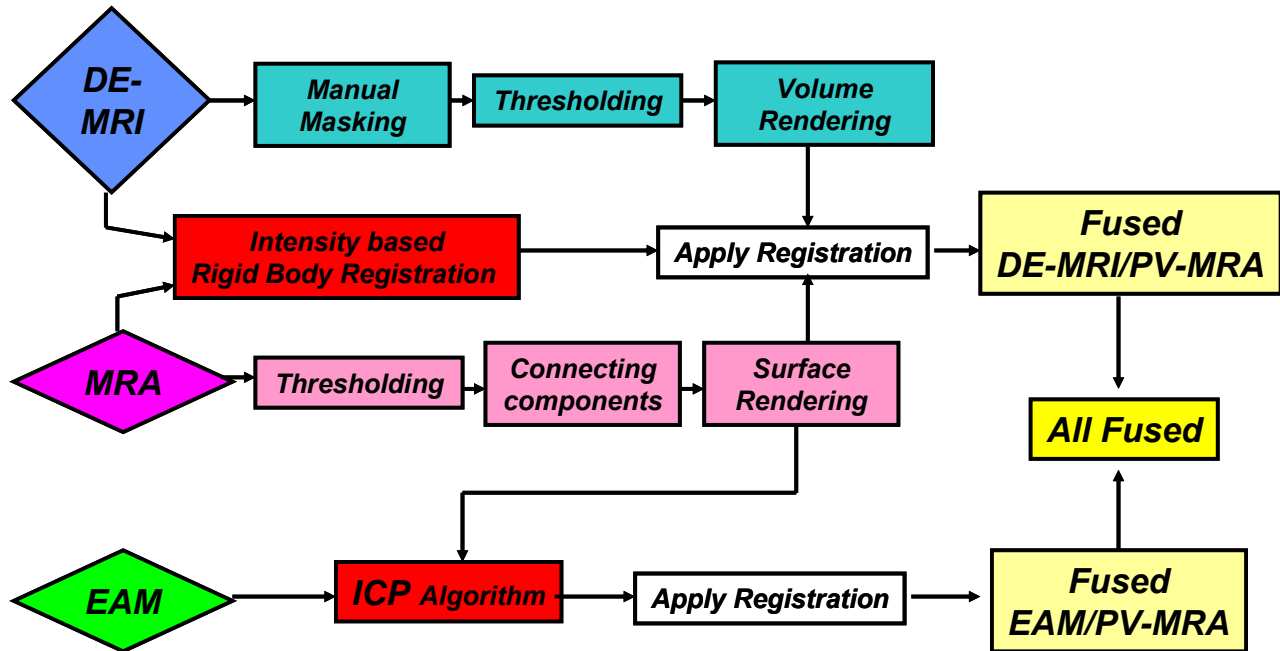


Figure 1. Registration methods for DE-MRI, MRA, and EAM data. Intensity-based rigid body registration was applied for the DE-MRI and PV-MRA registration. ICP was applied for PV-MRA and EAM data fusion.

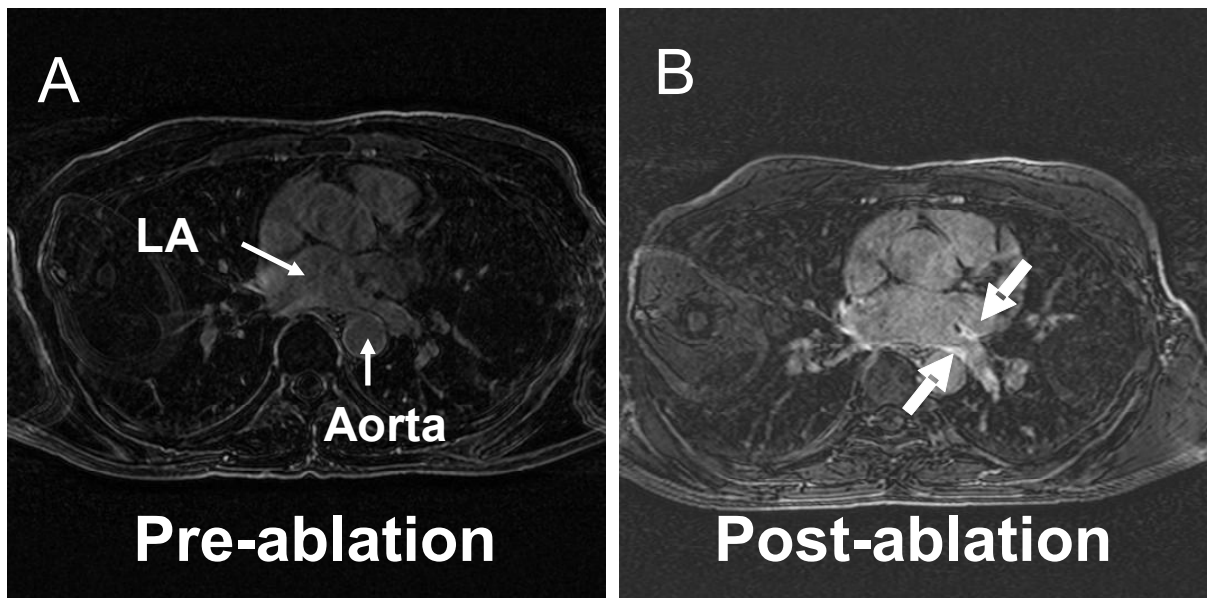


Figure 2 Pre(A)- and post(B)- ablation DE-MRI. A 3D navigator-gating (end-expiratory), and ECG-gated (end-diastolic) inversion-recovery segmented gradient echo sequence was performed 20 minutes after administration of 0.2mmol/kg of the Gd-DTPA injection. The scar tissue is enhanced.

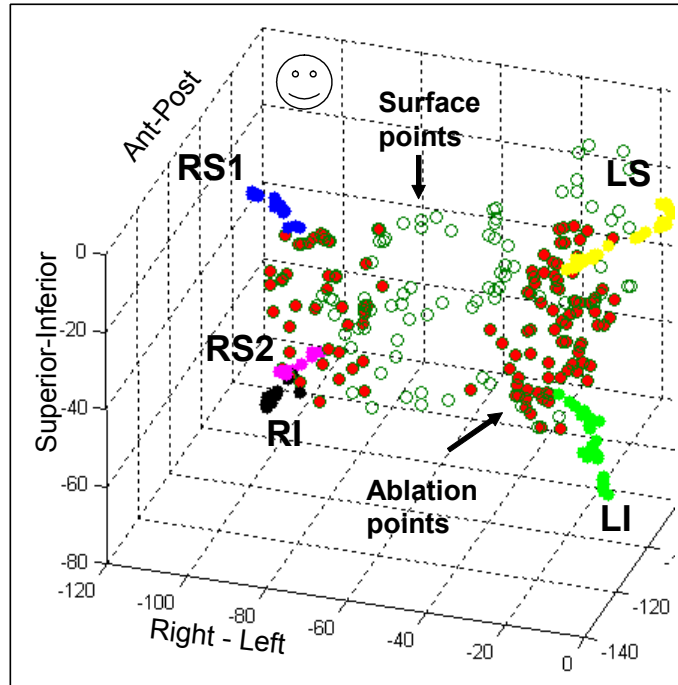


Figure 3 Raw EAM data displayed as point cloud, with x , y , and z coordinate obtained by catheter tracking. The major branches of the PVs and LA are shown as filled circles, and are labeled. The LA surface points are plotted as unfilled circles. The ablation sites are shown as red filled circles. The patient had five branches of PV (LI: left inferior, LS: left superior, RS1 and RS2: right superior, RI: right inferior).

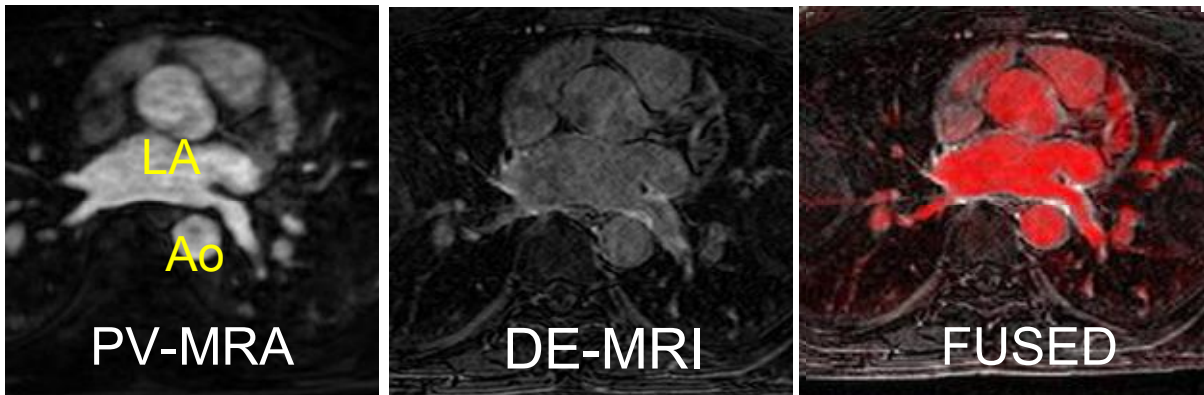


Figure 4 MRA and DE-CMR with different voxel sizes were fused by finding a rigid-body transformation between two image data sets by using intensity based rigid registration. LA: Left atrium; Ao: Aorta.

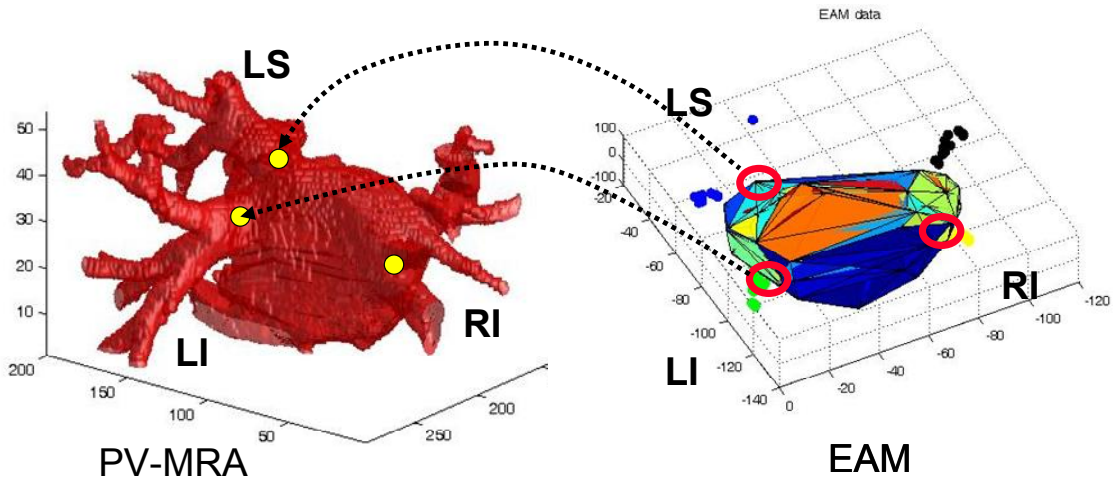


Figure 5 Landmark registration of PV-MRA and EAM data. Left superior (LS), Left inferior (LI), and Right inferior (RI) pulmonary vein (PV) were selected from both surface rendered PV-MRA and EAM data. SVD was applied to find transformation between these two data.

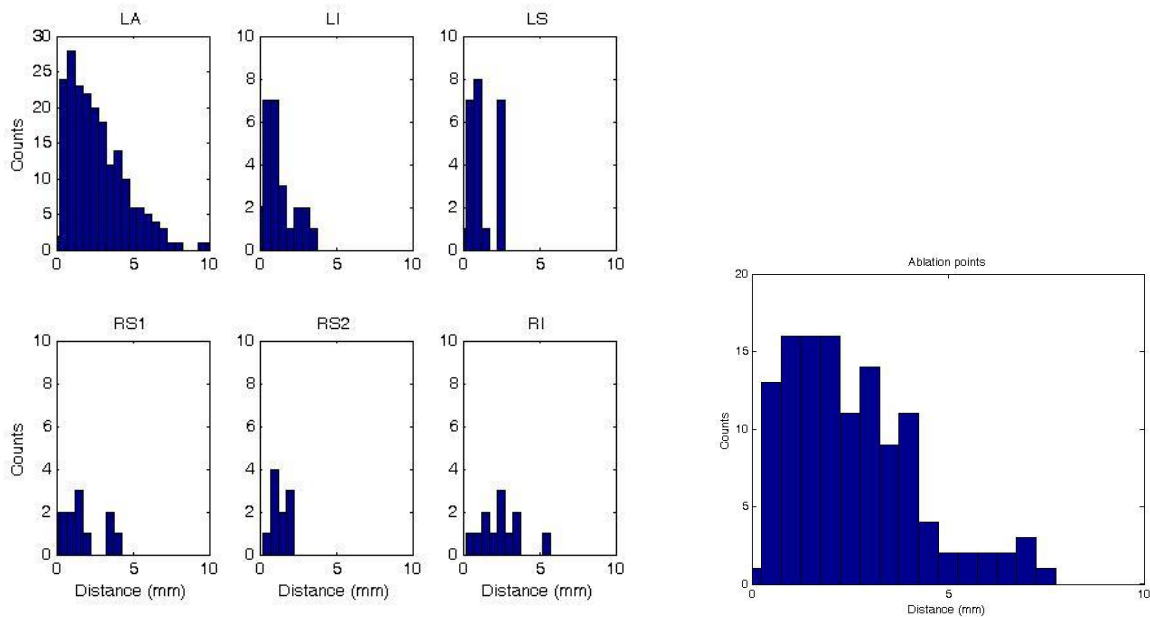


Figure 6 Histogram of distance between labeled LA, PV branches, and ablation points recorded by EAM and PV-MRA surface. LA: 2.8 ± 2.1 mm; LI: 1.3 ± 0.9 mm; LS: 2.7 ± 7.0 mm (without one outlier: 1.3 ± 0.8); RS1: 1.6 ± 1.3 mm; RS2: 1.2 ± 0.5 mm; RI: 2.5 ± 1.4 mm. Distance between PV-MRA surface to ablation points: Mean: 2.6 ± 1.7 mm. 50% of the points had less than 2.2 mm error, and 90% were within 4.7 mm.

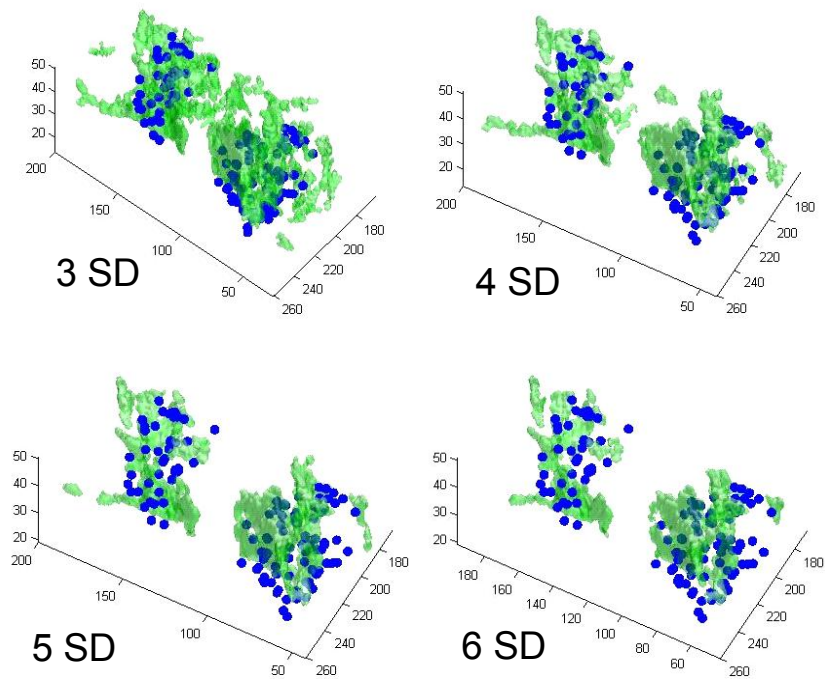


Figure 7 Ablation points and scar volume with different threshold (mean blood signal + 3, 4, 5, 6, STD). The scar volume is in green (gray). Blue dots (black) are ablation points. Scar surface with higher standard deviation dissociate from ablation points.

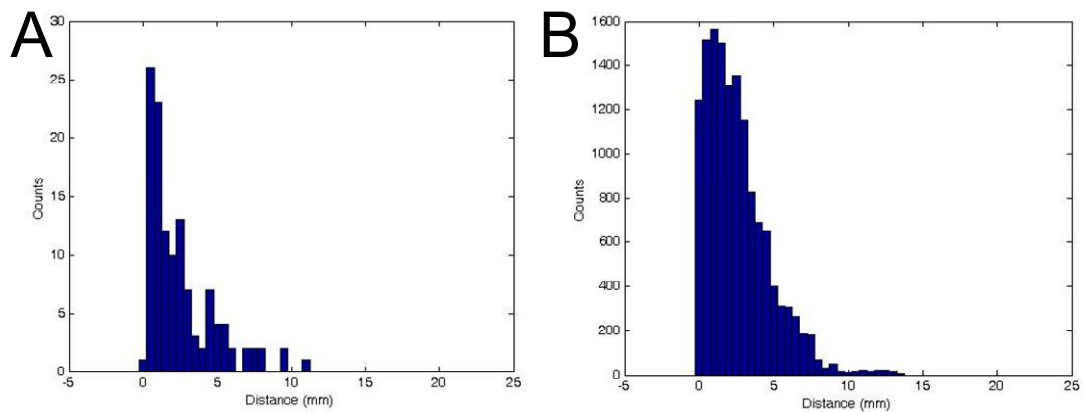


Figure 8 A: Histogram of distance between ablation points to scar surface (threshold at blood signal + 4STD air signal). Mean: 2.5 ± 2.3 . 50% of points had less than 1.7, and 90% of were within 5.5 mm. B: Histogram of distance between scar (threshold at blood + 4STD air signal) and PV-MRA surface. Mean: 2.6 ± 2.1 . 50% of points had less than 2.0 mm, and 90% of were within 5.5 mm.

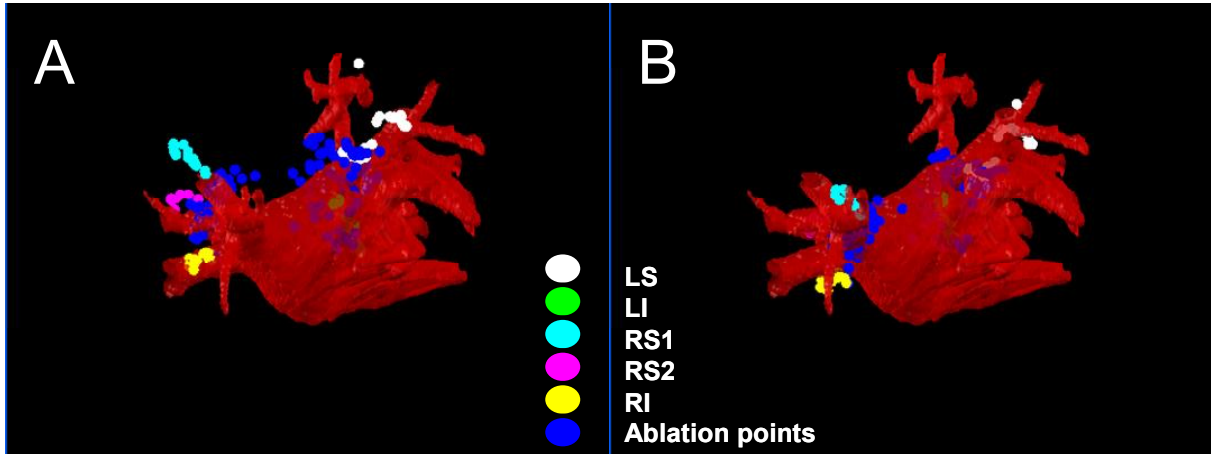


Figure 9 Landmark based registration and ICP registration. EAM data shown as dots, shaded form is segmented PV-MRA surface. (A) Initial coarse registration uses only ostial points of Left superior (LS), Left inferior (LI), and Right inferior (RI) pulmonary vein. After coarse registration, there is still PV ostia misalignment for branches not used for registration (e.g. Right superior (RS1 and RS2)). (B) After ICP, the PV ostial alignment is improved. PV branches are well aligned after initial landmark based rigid-body registration followed by ICP.

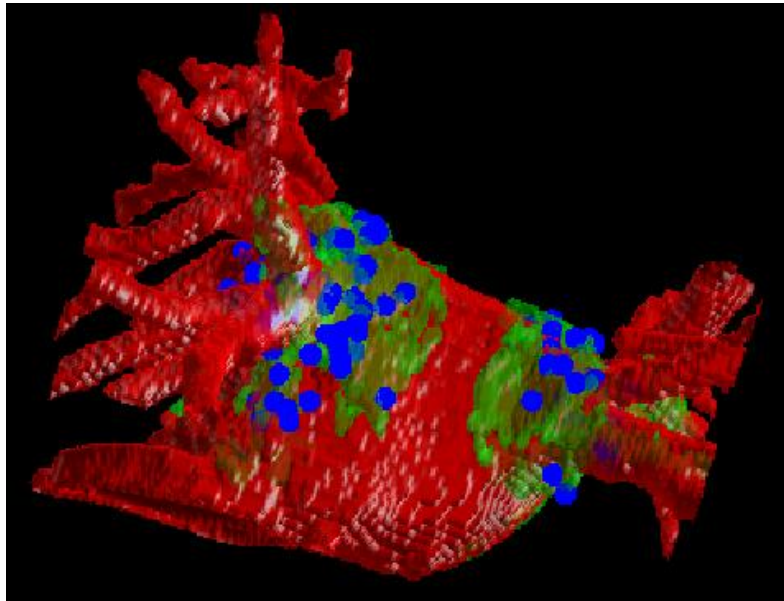


Figure 10. DE-MRI, PV-MRA, and EAM data were fused. Red Shell is the LA-PVs. Green area is scar form DE-MRI. Blue dots are ablation points.